Journal of
Synchrotron Radiation

ISSN 0909-0495

Received 6 February 2009
Accepted 3 April 2009

Real-time non-invasive detection of inhalable particulates delivered into live mouse airways

Martin Donnelley,[a]* Kaye S. Morgan,[b] Andreas Fouras,[c] William Skinner,[d] Kentaro Uesugi,[e] Naoto Yagi,[e] Karen K. W. Siu[b,f] and David W. Parsons[a,g,h]

[a]Respiratory and Sleep Medicine, Women's and Children's Hospital, Adelaide, Australia, [b]School of Physics, Monash University, Victoria, Australia, [c]Division of Biological Engineering, Monash University, Victoria, Australia, [d]Materials and Environmental Surface Science, University of South Australia, Australia, [e]SPring-8/JASRI, Hyogo, Japan, [f]Monash Centre for Synchrotron Science, Monash University, Victoria, Australia, [g]Department of Paediatrics, University of Adelaide, Australia, and [h]Women's and Children's Health Research Institute, Adelaide, Australia.
E-mail: martin.donnelley@adelaide.edu.au

Fine non-biological particles small enough to be suspended in the air are continually inhaled as we breathe. These particles deposit on airway surfaces where they are either cleared by airway defences or can remain and affect lung health. Pollutant particles from vehicles, building processes and mineral and industrial dusts have the potential to cause both immediate and delayed health problems. Because of their small size, it has not been possible to non-invasively examine how individual particles deposit on live airways, or to consider how they behave on the airway surface after deposition. In this study, synchrotron phase-contrast X-ray imaging (PCXI) has been utilized to detect and monitor individual particle deposition. The *in vitro* detectability of a range of potentially respirable particulates was first determined. Of the particulates tested, only asbestos, quarry dust, fibreglass and galena (lead sulfate) were visible *in vitro*. These particulates were then examined after delivery into the nasal airway of live anaesthetized mice; all were detectable *in vivo* but each exhibited different surface appearances and behaviour along the airway surface. The two fibrous particulates appeared as agglomerations enveloped by fluid, while the non-fibrous particulates were present as individual particles. Synchrotron PCXI provides the unique ability to non-invasively detect and track deposition of individual particulates in live mouse airways. With further refinement of particulate sizing and delivery techniques, PCXI should provide a novel approach for live animal monitoring of airway particulates relevant to lung health.

Keywords: particles; non-invasive; airway surface; X-ray phase contrast; asbestos; mouse; detection; X-ray imaging; radiography.

1. Background

Inhalation of pollutant particles starts immediately after birth, and the type of particles inhaled depends on the surrounding environment. Children can be unknowingly exposed to a wide range of potentially harmful particles of varied toxicity, ranging from established toxins such as asbestos and fibreglass fibres, lead fumes from smelters and (previously) motor vehicles, coal and mineral dusts from mines and quarries, to everyday dusts in the air. The lung size, airway physiology, breathing patterns and rapid development of young children significantly increases their risk over that of adults experiencing the same pollutant particle exposure (Wildhaber, 2006). Although the eventual effects on lung health from inhaling some of these particles are well known, particularly for asbestos (Addison & McConnell, 2008), no studies have examined the manner in which such particles deposit on airways, nor their physical behaviour and immediate fate after contacting the airway surface. Knowledge of particle deposition behaviour may help reveal factors that influence retention and thus the later pathophysiology in the lungs.

The ability of airways to clear inhaled particles *via* mucociliary transit is a clear diagnostic indicator of airway health. We are developing methods to monitor mucociliary transit in mice *in vivo* to assist in determining the effectiveness of genetic (Limberis *et al.*, 2002) and other potential therapeutics in cystic fibrosis airway disease. Although reliable methods for bulk detection of the clearance of particles in airways exist

(Grubb *et al.*, 2004; Donaldson *et al.*, 2007; Livraghi & Randell, 2007), respiratory science currently lacks a non-invasive method of detecting these individual particulates, or tracking their motion in real time. Knowledge of the behaviour of deposited particles in animal models may provide clues to the initiation of animal and human pathophysiology, and thus suggest potential preventative measures for use in young children as well as in adults. We therefore utilized novel synchrotron phase-contrast X-ray imaging (PCXI) to detect and monitor the deposition and comparative transit behaviour of representative pollutant particles in live mouse airways.

PCXI utilizes X-ray refraction in addition to conventional absorption to improve image contrast, and it is particularly useful for achieving soft tissue contrast where the absorption differences are small. Tissue boundaries are enhanced by the phase changes induced by differences in their X-ray refractive indices, provided the incident beam has sufficient spatial coherence and the sample-to-detector distance is sufficiently long (Snigirev *et al.*, 1995; Cloetens *et al.*, 1996; Wilkins *et al.*, 1996). We have already shown the ability of PCXI for non-invasive airspace imaging in small animals (Parsons *et al.*, 2008). The aim of this study was to test the capability of PCXI for non-invasive particulate detection in live mouse airways.

2. Methods

The experiment first utilized an *in vitro* study to determine which of a range of biologically relevant particulates were detectable using synchrotron PCXI. For those particles that were adequately detectable, we then examined their *in vivo* behaviour when deposited on live mouse airways.

The experiment was performed on the undulator beamline BL20XU at the SPring-8 Synchrotron Radiation Facility, Hyogo, Japan. The imaging hutch was located 245 m from the storage ring in the Biomedical Imaging Centre, and the imaging layout was as shown previously (Parsons *et al.*, 2008). Monochromatic X-rays of 25 keV (λ = 0.5 Å) were selected using a standard double-crystal monochromator (Yabashi *et al.*, 1999). At the imaging station the beam size was approximately 10 mm (H) × 6 mm (V) and the incident photon flux was approximately 4.37×10^9 photons s^{-1}, producing an estimated dose rate of 0.61 Gy s^{-1}. The propagation (sample to detector) distance was 135 cm, chosen to produce a sufficiently strong bright/dark fringe from each particle, so that they could be identified amid intensity variations introduced by overlying tissue and skin. Images were captured using a high-resolution X-ray converter (10 mm maximum diameter field of view; AA50 Hamamatsu Photonics) with a charge-coupled device (CCD) detector. The converter used a 10 µm-thick scintillator (Lu_2SiO_5:Ce) to convert X-rays to visible light, which was then directed to the CCD using a ×20 X-ray converter microscope objective lens with a numerical aperture of 0.4. The detector was a pco.4000 (PCO Imaging) with an array size of 4008 × 2672 pixels and a 9 µm native pixel size. This set-up resulted in an effective isotropic pixel size of 0.45 µm and a field of view of 1.8 mm × 1.2 mm. The FWHM of the point spread function, as determined from a horizontal edge image, was measured at 3.6 µm. Exposure times between 90 ms and 300 ms were used for the *in vitro* studies, and 300 ms for the *in vivo* studies.

2.1. *In vitro* studies

A range of potentially respirable pollutant particles were examined dry or suspended in a carrier fluid (distilled water) to determine their visibility using PCXI. Chrysotile (white asbestos), provided by the South Australian Museum, and fibreglass from a commercial pipe insulation were separately ground under water to produce fibres suited for examination. Galena, the natural mineral form of lead sulfide (PbS), was also obtained from the South Australian Museum, and dolomite quarry dust was provided courtesy of the Boral Resources (SA) Limited Linwood Quarry, Adelaide, South Australia. Other relevant compounds, tested to confirm, in part, theoretical limitations in the application of PCXI imaging, included combusted diesel particles and standard roadside PM10 filtered particulate matter (provided by Dr I. Gilmour, USA EPA, Research Triangle, NC, USA), and laser printer toner (Epson).

All particle samples (except asbestos, see *Results*) were sieved using a 25 µm × 25 µm orifice stainless-steel mesh; a small sample was then tapped, puffed or dropped onto the exposed adhesive surface of short lengths of Kapton tape, a polyimide film highly transparent to X-rays (PC500 1 µm-thick with 1.5 µm-thick silicon adhesive; Argon Masking Inc.). The particles were then sealed in place using a second piece of tape. The samples were mounted on a controllable *XY* stage in the hutch for imaging. Comparative images taken under light microscopy at ×400 magnification were also used to ensure the regions imaged using PCXI included the particles of interest.

2.2. *In vivo* studies

For the *in vivo* experiments, ten hairless mice (Crlj:CD1-*Foxn1*^{nu}) weighing ∼18–26 g were imaged under approval from the Animal Ethics Committee of SPring-8 and of the Children, Youth and Women's Health Service, Adelaide. Mice were anaesthetized with Nembutal (45 mg kg^{-1}, i.p.) and were humanely killed *via* Nembutal overdose (500 mg kg^{-1}, i.p.) at the end of each study without awakening. The anaesthetized mice were secured on a polyethylene imaging board containing an open slot to allow the passage of the X-ray beam directed anterior to posterior along the centre line of the mouse. The dorsal incisors were hooked over a stainless-steel wire loop, and the limbs and shoulders, and above and below the imaging area in the head, were taped to minimize body movements owing to respiration during imaging. The level of anaesthesia was monitored by foot pinch and changes in respiration. Nembutal was continuously infused by a syringe pump *via* an indwelling i.p. needle (typically at a rate of 0.9 µl min^{-1}), with additional top-up Nembutal injections given as required.

A small-diameter polyethylene recording cannula, made from heat-pulled and thinned polyethylene PE10 tubing (Tyco

Electronics), was placed to a depth of 10 mm in the right nostril, to provide a route for direct delivery of test particulate agents suspended in water to the nasal airway. The position of the cannula tip in the nose was recorded at the end of several deposition studies by inserting a fine wire, previously aligned to reach to the end of the cannula tip. The distinctive bone suture line in the nasopharyngeal airway posterior to the olfactory region provided an easily locatable landmark near which the airway imaging was performed (Fig. 2). Nasal airways in laboratory mice were utilized here since they are commonly used as a model site for pre-clinical testing of airway function after gene transfer procedures by our group (Limberis *et al.*, 2002) and others (Grubb & Boucher, 1999). The mouse nasal airway is lined with the ciliated respiratory epithelium which mimics that present in human lung conducting airways. This region is also well suited to these first live PCXI particulate imaging procedures because the airway is stable within the head and shows little movement during breathing; in contrast, lung airways are in almost continuous motion during breathing.

Images were captured at a rate of 0.2 Hz. After 1 min of baseline collection, samples of particulates suspended in distilled water were delivered *via* the nasal cannula either manually or using a syringe pump, at volumes between 15 µl and 50 µl, in one bolus over 10 to 60 s (see *Results*). Image collection was continued at 0.2 Hz for a further 19 min, creating a dataset consisting of 240 images, close to the maximum number of images (260) the pco.4000 camera's onboard memory buffer could record.

The anatomy of the mouse head at the imaging location introduced confusing detail (from other head structures in the path of the X-ray beam) into the PCXI images, which could obscure individual small particles in single images. To facilitate rapid and accurate location of relevant particles, each image sequence was analysed with simple motion-detection software (*VirtualDub*, Version 1.8.6, Avery Lee, using the MSU Motion Estimation plug-in, Graphics and Media Lab, Moscow State University) to reveal where motion was occurring by applying digital image subtraction and filtering algorithms that identify regions of the image that change between frames. The output of this motion-detection software was sequential frames that were neutral grey where there was no motion detected, and lighter or darker grey where motion was detected. The dark outlines corresponded to the most recent position of the moving object, and the light outlines corresponded to the position of the object in the previous frame. For high-quality motion detection the background must remain still compared with the moving objects to be detected, hence the special efforts we made to minimize the movement of the mouse during imaging.

3. Results

3.1. *In vitro* studies

We first tested the range of potential pollutant or toxic particles encapsulated between adhesive Kapton tape and examined their detectability under PCXI, prior to use in live mice. At a propagation distance of 135 cm, many particles were visible both from phase contrast or absorption, or a combination of both. For example, galena absorption dominated the image contrast, and thus produced shadows with no fringes. In contrast, the glass beads refracted the X-rays and introduced variations in the phase of the X-ray wave across the width of the object. The interference of the phase-shifted waves produced light and dark fringes, *i.e.* phase contrast, but not a dark shadow where the glass was, since it did not absorb strongly. Some particles, such as quarry dust, showed both phase and absorption contrast, appearing darker where the object attenuated the beam, as well as having some bright/dark fringes around the edges. The 300 ms exposure length produced the optimum images, capturing sufficient incident photons to fill the potential dynamic range (2^{14} grey levels), thus providing the maximal signal-to-noise ratio without inducing detector saturation. Fig. 1 shows results of these *in vitro* studies, and clearly demonstrates the differences in detectability between particle types.

Small individual asbestos fibre bundles, ranging in width from 4 µm to 15 µm and in length from near 25 µm through to several millimetres, could be seen in the PCXI images (Fig. 1*a*). Additionally, many large fibre bundles were also present, some with widths up to 200 µm, as observed under light microscopy. Despite extensive manual wet-grinding, asbestos particles could not be ground and separated into uniform size fractions. In addition, asbestos ground under water formed an enmeshed fibrous meshwork that resisted centrifugation (6500 r.p.m. up to 5 min) or extended ultrasonification (up to 10 min) that should have assisted in its preparation into finer diameter fractions. For safety reasons, in this study we did not attempt to employ dry grinding to produce smaller dry asbestos fibres. As a result, the delivery of asbestos was technically difficult because large fibres could clog the cannula tip when the fluid dose was drawn into, or ejected from, the dosing cannula. Thus we relied on settling in water in an attempt to obtain finer size fractions. Nevertheless, clumps of fine fibres could still be observed when samples were ejected onto a clean surface, suggesting that asbestos fibre clumps could still occur when delivered *via* a cannula.

Like asbestos, quarry dust was also readily detectable (phase and absorption contrast) but appeared as compact irregularly shaped particles primarily between 7 µm and 30 µm. Although particles (apart from asbestos) were sieved through a 25 µm square stainless-steel mesh, occasional larger particles (up to 90 µm) were also present (*e.g.* Fig. 1*b*) possibly owing to clumping effects. The quarry dust produced more image contrast than the asbestos (but significantly less than galena, see below).

Fibreglass was substantially less visible than either asbestos or quarry dust (phase contrast and absorption). Under PCXI the fibreglass particles had the same individual fibre/rod morphology present in light microscopy (Fig. 1*c*). Most fibres were between 12 µm and 25 µm in length, but again there were a small number of fibres with lengths up to 100 µm. Unlike asbestos fibres there was little variation in fibre width, with all

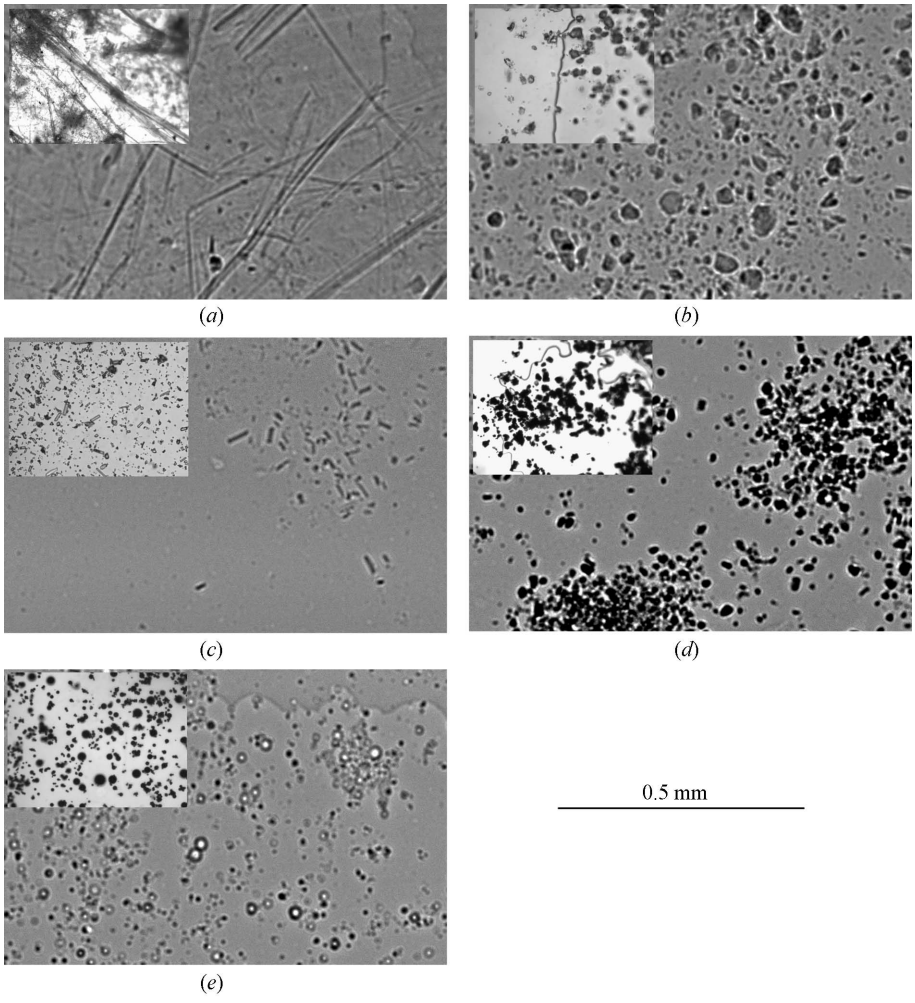

Figure 1
In vitro dry particulate testing revealed the particulates that were visible using PCXI. Samples were examined under PCXI (main pictures) and light microscope (insets): (*a*) asbestos, (*b*) quarry dust, (*c*) fibreglass, (*d*) galena and (*e*) silver-coated hollow glass beads. The morphology of each of the particulates is clearly very different. For layout and presentation purposes, and so they are at the same level of magnification, the PCXI images are cropped to 0.90 mm × 0.60 mm, and the light microscope images are 0.365 mm × 0.27 mm.

visible fibres approximately 8 μm wide. Similar to asbestos, fibreglass fibres used here were normally longer than 100 μm, but unlike asbestos the grinding process was effective for reducing the length of the fibres. We did not observe an enmeshed network when examining the fibreglass samples and there was no difficulty drawing or expelling the fibreglass samples in solution *via* the thin cannula.

Samples containing lead were obtained by grinding galena (PbS). Not surprisingly, these particles were easily detected under PCXI, primarily *via* absorption, and appeared similar to images obtained under light microscopy (Fig. 1*d*). The galena particles ranged in size from 10 μm up to 30 μm, and in comparison with the quarry dust they were denser, more uniform in shape, and were less varied in size. Since all samples were prepared as a percentage *w*/*v*, the galena samples contained fewer particles per volume owing to the higher density of the mineral; nevertheless, there were sufficient particles present for *in vitro* detection.

We have routinely employed silver-coated hollow glass beads as PCXI markers (Fig. 1*e*) because the air within the bead provides good visibility under PCXI. This is due to the enhanced phase-contrast effect from the high-refractive-index gradient across the glass–air boundary, despite the material producing little absorption. In both the PCXI and light microscopy images the beads were easily detected, with diameters varying between 12 μm and 25 μm despite the stated nominal diameter being 14 μm. Under light microscopy all the beads appeared solid, because the silver coating makes them opaque to visible light. However, under PCXI most beads appeared hollow because the air within them refracted the X-ray beam so that they showed up more clearly with phase contrast. Some of the smaller beads present were not hollow, and so produced little phase contrast.

At the completion of the *in vitro* testing, five particle types were considered sufficiently visible to warrant study *in vivo*. Not all particles detected *in vitro* were suitable because the mouse head structures surrounding the airway being imaged would obscure particulates that were poorly visible *in vitro*. For *in vivo* study we selected the fibrous particulates asbestos and fibreglass, and the non-fibrous quarry dust and galena. We also used silver-coated hollow glass beads as reference particles. The largely carbon-based particulates, combusted diesel, PM10 and laser printer toner, were not sufficiently visible to warrant *in vivo* testing.

3.2. *In vivo* studies

3.2.1. Site of particulate delivery in mouse airway. The 10 mm delivery depth of the nasal airway cannula placed the tip just anterior to the origin of the nasopharyngeal airway (Fig. 2). This location was approximately 5.5 mm anterior to our standard nasopharyngeal imaging region near the skull-bone suture line (Parsons *et al.*, 2008) that is readily located in each animal.

3.2.2. Determination of dosing protocol. Based on the *in vitro* studies, an initial testing protocol for use in live mice was created to achieve maximal use of each mouse and the limited beam time available. After a brief baseline imaging period (no treatment), each animal received one of the fibrous particle instillations (either asbestos or fibreglass), along with the reference hollow glass beads. The instillation was

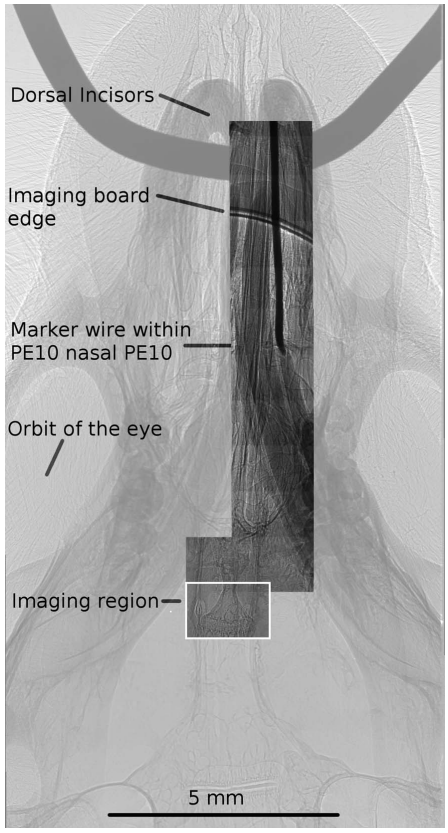

Figure 2
A montage of 13 individual adjacent and offset PCXI images showing the cannula position and the imaging location (white square), overlaid on a larger general PCXI image of the whole mouse skull (taken from Parsons *et al.*, 2008). The fine-gauge wire reaching to the cannula tip is apparent (the cannula itself cannot be discerned at this magnification). As shown here, the tip is located at the rear of the olfactory region. The plastic restraint board used in these latter studies included a cut-out region; the curved edge of this opening is noted. For additional anatomical landmarks, see Parsons *et al.* (2008).

performed remotely over 60 s using a syringe pump (dose volumes as determined below). Approximately 25 min later one of the non-fibrous particulates (either galena or quarry dust) was delivered manually over 10 s; manual solution changes required opening of the imaging hutch for physical access to the instillation syringe by the experimenter. This protocol ensured that all particulates could be tested using a small number of mice, while the simultaneous delivery of the control particles (glass beads) was used to confirm that successful instillation had occurred.

3.2.3. Effect of particulate delivery volume, rate and concentration. Based on the overall particulate density seen in the *in vitro* PCXI images, concentrations of 0.5% *w*/*v* for fibreglass and asbestos (mixed with 0.5% *w*/*v* reference glass beads) and 0.1% for galena and quarry dust were chosen, to provide a sufficient quantity of particulates to be visible *in vivo*, but to limit the possibility of cannula or airway blockage during deposition.

Initially the volume was set at 50 µl delivered over 10 s, replicating the tolerable dose volume typically used when dosing the mouse lung *via* the nasal airway. This combination was tested in one mouse. Fluid and particles were detected immediately after dose delivery began. However, the 50 µl volume produced a period of cough-like respiratory excursions that, while small and transient, caused sufficient body movement to produce blurring of some captured images. These factors suggested that smaller doses delivered over a longer period should be trialled to minimize movements caused by the dosing protocol, while retaining the ability to detect particles in the nasal airway.

Accordingly, the dose volume was progressively reduced in two subsequent mice. We found that a 15 µl dose volume provided sufficient visible fluid and particulates to be monitored in the nasal airway, but induced only a brief increase (< 1 min) in respiratory effort. Importantly, subsequent dosing in the same animal was also well tolerated with this dose volume. For the fibrous particulates the 15 µl dose was delivered by syringe pump over a period of 60 s, commencing after the initial 60 s of baseline imaging. As the galena and quarry dust particles settled more rapidly, these were manually instilled over a period of approximately 10 s. This protocol was used for the seven remaining animals.

3.2.4. Particulate detection. Using the motion-detection software all five particulates could be detected *in vivo*, although with different degrees of visibility and with varying levels of difficulty. On the airway surface the fibrous particulates were surrounded with fluid; since this was of similar refractive index to these particles it resulted in a reduction in phase contrast and a loss of particle visibility within the fluid envelope. Thus *in vivo* detection of all particles (other than the hollow glass beads) was more reliant on absorption contrast than phase contrast.

For both fibrous particles an initial bulk liquid dose moved past the imaging site within approximately 90 s after the start of dose delivery. The rapid movement coupled with relatively long exposure times meant that we could not determine whether particulates were contained within the moving liquid. Because the heavier non-fibrous particulates (galena and quarry dust) were delivered manually and there was a delay (typically 1 min) between particulate delivery and imaging, during which the beamline hutch was closed and the X-ray shutter was opened, we were unable to determine whether an initial bulk movement of the dose liquid was present immediately after delivery.

Compared with the number and size of the particulates detected *in vitro* (Fig. 1), very few large particulates were seen *in vivo* (Figs. 3–7). Large particles that were detected took longer to appear at the imaging site than the small particulates. Additionally, in some animals asbestos fibres took 4 to 5 min to appear. In comparison, all other particulates appeared within 1 min of commencing instillation (or as soon as imaging could be started in the case of the galena and quarry dust).

The rate at which the different particulate types moved along the airway varied widely, between 0.1 mm min^{-1} and 4.4 mm min^{-1}. When examining the non-fibrous particulates, a small number of fibrous particulates from the first part of the dosing protocol 30 min beforehand continued to move past the imaging site. However, the different appearance of each

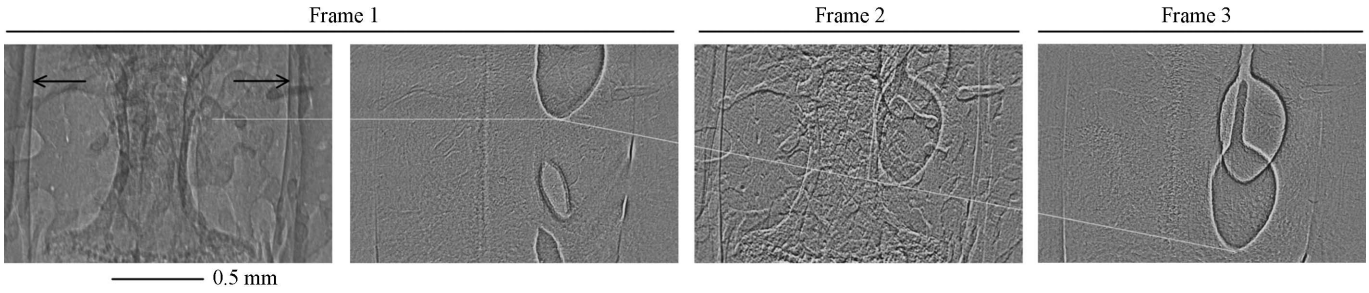

Figure 3
Asbestos particulate detection. The two panes on the left show the original PCXI image and its corresponding motion-detected frame that revealed the moving object on the airway. The panes on the right are the next two motion-detected frames in the sequence. The black arrows mark the nasal airway edge running vertically through the image, and the white lines follow the same object across the three sequential frames each separated by 5 s. The last frame shows an enveloped clump of fibres with an elongated tail. These enveloped structures moved along the airway faster than all other particles studied, here at a rate of 4.4 mm min^{-1}.

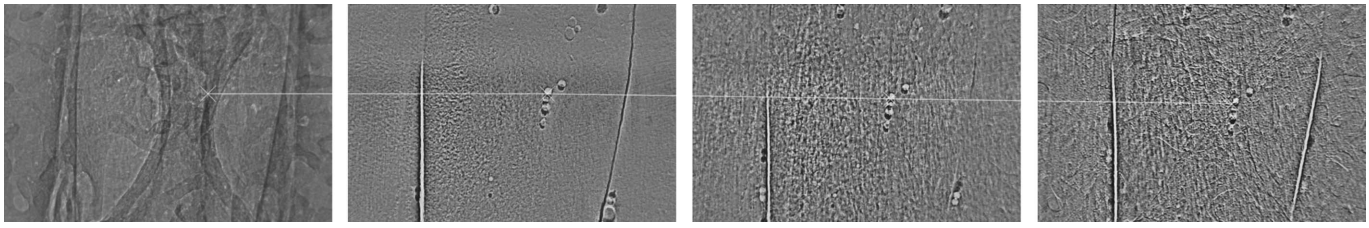

Figure 4
Four particles of quarry dust are visible at the centre of the motion-detected frames. Particles did not aggregate or have the appearance of trapping liquid around them on the airway surface. In this sequence the quarry dust particles are moving at a rate of 0.41 mm min^{-1}.

particle type in the airway ensured that they could still be differentiated.

3.2.5. Appearance of particulates in live mouse airway. *Asbestos.* Fig. 3 shows the appearance of asbestos fibres as revealed using the motion-detection software (see *Methods*). In this and all other *in vivo* images presented here, the first frame is the raw PCXI image and the second is its corresponding motion-detected frame. On the right are the next two motion-detected frames captured 5 s and 10 s, respectively, after the original frame. Interestingly, the third pane in Fig. 3 shows more background detail because a slight movement of the mouse head was picked up by the motion detection. Unlike in the *in vitro* study, individual asbestos fibres were not detected, but appeared as agglomerations of enmeshed fibres trapped in liquid. The enveloped structure could be seen moving along the airway. We noted that there were few of these agglomerations present, but where detected they were large compared with the sizes of the individual fibres, in some cases up to 1 mm in length. These structures moved more rapidly *in vivo* than the other particulates. The sequence in Fig. 3 shows the unusual shape of these airway surface structures which often possessed a 'tail' that trailed behind the fluid envelope.

Quarry dust. The quarry dust was also readily detectable *in vivo* (Fig. 4) where it appeared as compact and irregularly shaped particles. The smallest detectable dust particles were approximately 10 µm, but, unlike in the *in vitro* study where large particles up to 90 µm diameter were present, most *in vivo* particles were smaller, less than $\sim$50 µm. While the quarry dust particles produced a greater image contrast than that seen with asbestos, there was no appearance of aggregation; the dust was only present as individual particles and did not show a fluid envelope when detected on the airway surface.

Fibreglass. Although fibreglass was substantially less visible than either asbestos or quarry dust *in vitro*, it was readily detectable *in vivo* (see Fig. 5). Fibreglass fibres displayed the smooth, enveloped, but irregularly shaped form similar to that seen with asbestos. Individual fibres were generally not visible, thus we could not determine a minimum detection size. These enveloped fibreglass shapes moved at approximately one tenth of the rate of the larger asbestos objects.

Galena (PbS). Despite its high density, galena was difficult to detect *in vivo*. The particles were smaller than quarry dust and did not provide strong phase contrast (*i.e.* detection appeared to be *via* absorption only) (Fig. 6).

Hollow glass beads. As noted above, the air contained within these small beads enhanced their visibility owing to phase contrast. When delivered concurrently with the fibrous particulates they were visible (albeit sometimes in low numbers) in many images (Fig. 7). Like galena and quarry dust, the hollow glass beads appeared as individual particles and their appearance did not indicate that a liquid envelope was present whilst moving along the airway surface.

4. Discussion

The primary goal of this study was to determine whether the refractive (phase) and absorption characteristics of common pollutant particles permitted their detection in live mouse airways using synchrotron PCXI. The *in vitro* results showed

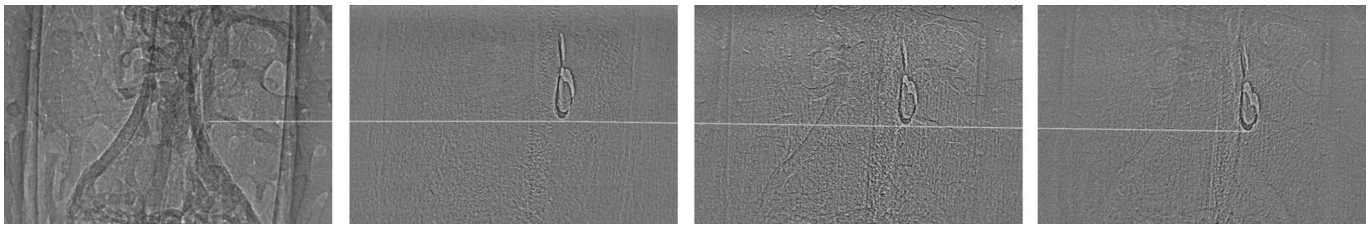

Figure 5
Fibreglass appears similar to asbestos, but the objects were smaller and had shorter tails. Like asbestos, the fibres appeared to smoothly trap liquid around them so that individual fibreglass fibres could not be seen. Fibreglass moved at the same speed as the quarry dust, at 0.41 mm min^{-1}.

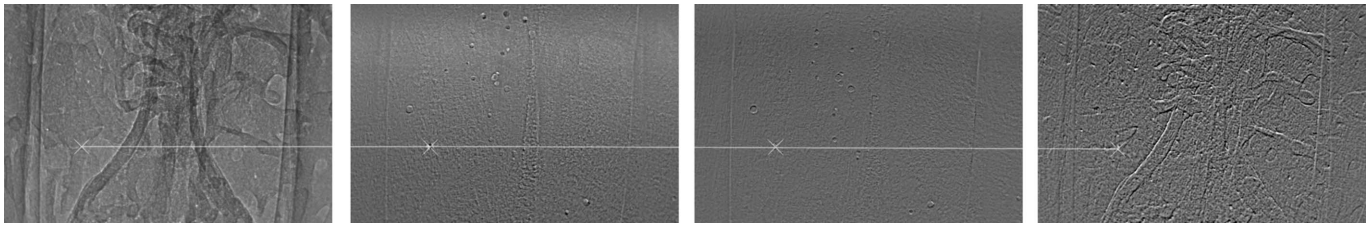

Figure 6
Galena particles were the most difficult to locate in the *in vivo* PCXI images, and also moved the slowest, at 0.1 mm min^{-1}.

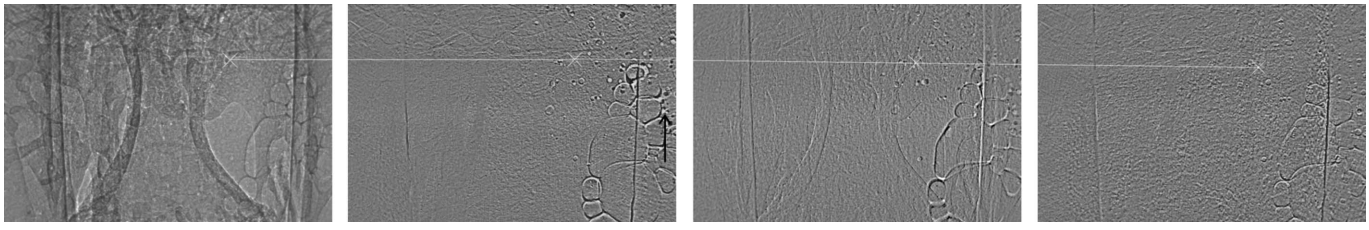

Figure 7
Reference hollow glass beads. In this animal, beads are located in the nasal airway, but also in the mouth (black arrow to the right of the right-hand-side airway edge). The glass beads moved in the nasal airway at 0.3 mm min^{-1}.

that the PCXI technology was well suited to the detection of asbestos, quarry dust, fibreglass and galena as raw particulates.

To our knowledge this is the first report of the ability to detect and monitor the surface behaviour of these pollutant particles, non-invasively, in live airways. This capability is significant because PCXI has the unique ability to image the initial deposition, airway surface appearance, and the movement characteristics of individual particulates on an intact live airway surface. Furthermore, this approach has provided new information about the behaviour of individual particles of potential significance in studying respiratory disease from the earliest points of interaction in the airway, at times far earlier than previously possible.

Our ability to use *in vivo* PCXI imaging during the actual instillations of particulates, *via* a remote-controlled syringe pump, demonstrated that a volume of 15 µl was sufficient to produce detectable particulates in the nasal airway, and that this dose setting ensured there were minimal respiratory side effects able to cause movements that blurred subsequent image captures. These side effects may have been greater than normal because mice were imaged in a vertical orientation, whereas mice are normally studied supine or prone when anaesthetized in biomedical studies. Gravity may also have impeded clearance of instilled fluid that reached the lung, causing higher than normal cough and respiratory excursions.

In general, there were smaller numbers of particulates detected than expected, given the concentration and volume delivered. Some of the delivered volume may have been trapped in the tortuous olfactory passages present in mice, and it is not possible to know the exact location of the cannula tip in this complex organ [see Mery *et al.* (1994) for anatomical details] when introduced *via* the nose (Parsons *et al.*, 2008). More frequent detection of particulates could occur if the particle concentration was higher, especially for galena and quarry dust. However, 0.1% *w*/*v* is the common standard dose concentration for fluid-based instillations in mouse models, when testing the effects of atmospheric particulates on airway and lung health (I. Gilmour, personal communication). Accordingly, use of higher particle concentrations [as a percentage (*w*/*v*)] would not align with accepted practice. We believe that better targeting of cannula tip, confirmed by placement *via* orthogonal imaging at the commencement of PCXI studies, will improve nasal as well as lung delivery when using small dose volumes.

Although individual asbestos and fibreglass fibres were not visible *in vivo*, both fibres appeared to attract a liquid

envelope around them when observed on the airway surface. In contrast, galena and quarry dust remained visible as individual particles. The fibreglass particle agglomerates were smaller than for asbestos, presumably owing to the much shorter particle lengths created by the grinding process. Asbestos fibres naturally aggregate through hydrogen bonding, depending on the relative exposure of their hydroxylated surfaces, either in the natural mineral or after extended exposure to water (Healey & Young, 1954; Pundsack, 1955). Our inability to grind the asbestos under water (Papirer & Roland, 1981) to produce uniform suspensions of smaller fibres supports this interpretation. In this setting we interpret the objects found transiting the airway surface after dosing as enmeshed asbestos fibre clumps enveloped with fluid, and this interpretation is supported by the similar structures present after fibreglass fibre delivery. Furthermore, both types of fibres clumped such that in many cases an enclosed 'tail' followed behind the direction of movement of the object. Although we could not detect individual fibres within these objects, it seems likely that these tails contained fibres that extended behind the core meshed clump of fibres as it moved along the airway surface.

Since we never observed individual asbestos fibres on the airway we could not determine the size of the delivered fibres or the minimum size of asbestos fibres that were detectable *in vivo via* PCXI. The high rate of movement of these objects, much larger than both the similar fibreglass-based objects and the other individual particles, raises the possibility that airways deal with the deposition and transport of fibre-based particles on live airway surfaces *via* a fundamentally different mechanism to that underlying deposition of non-fibrous particles like dust and galena. Inhalation of asbestos can have devastating health consequences on lung health, and further study of the way that airways handle such fibres when they are first encountered may provide new insights into the earliest pathophysiological components of asbestos lung disease.

Galena was difficult to detect *in vivo* despite its high density because it was the smallest of all the particles, and there were fewer particles present (on a *w*/*v* basis). We also noted that galena particulates rapidly settled out of the delivery fluid, reducing the delivery effectiveness from the dosing cannula. In addition, because of the imaging delay after manual instillation and the upright orientation of the mouse, some of the heavier particulates may have already passed the imaging site by the time imaging commenced, especially if carried within a large initial bolus that would likely have been produced by delivery over the shorter instillation time of 10 s. Smaller galena particles could also be mistaken for the small dark spots present in baseline images and probably caused by individual or overlaid phase-contrast edge-enhancement effects derived from the various skull-bone fine structure encountered by the X-ray beam as it transits the head. Accordingly, we propose that it is essential to analyse these image sequences using motion-detection routines so that only moving particles were detected. Galena also produced little phase contrast and it did not trap an envelope of liquid around it. We speculate that the absence of a liquid layer around the galena, quarry dust and glass beads could also in part be due to the interaction between their shape and the local surface tension environment on the airway surface.

To our knowledge this is the first study to examine PCXI detection of individual particles *in vivo*, and there are a number of limitations inherent in the techniques and the interpretation of the results we have provided. While our findings are novel, use particles relevant to respiratory health (excluding the reference hollow glass beads) and show the potential of PCXI for studying live mouse airways, the nature and controllability of the particulate doses is not yet optimal, and the normal exposure and uptake of those particulates is quite different.

Firstly, the effective (aerodynamic) diameter of inhaled particulates must be less than approximately 10 µm to be capable of inhalation past the oropharynx, into the lung of humans. Fibres and particles below approximately 1–2 µm in diameter can be inhaled into the deepest parts of the lungs (Miserocchi *et al.*, 2008) while larger sizes such as the >7 µm fibres we examined *in vitro* would contact the conducting-airway walls and be removed by mucociliary clearance and coughing. An improvement in the minimum size detectable under PCXI will be important for ensuring biological relevance in future instillation or inhalation studies, especially with the growing awareness of the importance of ultrafine (<2.5 µm diameter) particles. Secondly, the lead-containing particles were ground galena which is a form of lead different to that inhaled as lead fumes (*e.g.* lead sulfates or oxides) from a lead smelter or in leaded petrol. Finally, for fibreglass there are many forms and uses of this fibre, and the type of fibreglass we used (from pipe lagging) may not be representative of that producing exposure at health-affecting levels in industrial or residential settings.

Although convenient experimentally, delivering particles into mouse airways within a distilled water bolus is not usual in life; inhalation as an aerosol or a dry powder is more physiologically relevant, and planned studies will examine this particle delivery approach. The methodology we used, though effective, also warrants improvement if PCXI is to become a useful technique in respiratory research. While the skull-bone suture line is easy to locate in the mouse nasal airway and produces a repeatable and stable imaging location under PCXI, we are now examining effects in lung airways since this is the relevant target organ.

Despite some difficulty detecting and tracking particles in the raw image sequences, moving particulates could be readily revealed using motion-detection processing. Unfortunately motion-detection analysis is not suited to detecting stationary particles. However, from our experience we propose that such analysis will be essential when performing such *in vivo* non-invasive studies of airway particulate deposition.

In these first studies little effort was made to limit radiation dose, which was too intense to consider animal recovery and repeated imaging. The current rapid development of synchrotron and imaging technology suggests there will continue to be improvements in CCD sensor technology, and analytical techniques such as motion detection and particle

tracking. Combined, they should lead to improved image resolution and higher light sensitivity, allowing smaller, and therefore more physiologically relevant, particulates to be detected and tracked. Minimizing tissue motion *via* combined respiratory and cardiac gating (Sera *et al.*, 2008) will reduce blurring and motion artefacts and result in more usable images. These gradual improvements should result in better particulate visualization to permit deposition and detection of smaller particulates, as well as shorter exposure times that both minimize motion artefact and produce essential reductions in radiation dose. However, despite these needs for improvement there are no imaging alternatives that can non-invasively detect and track such small and individual particles or fibre clusters *in vivo*, and these PCXI techniques should provide a novel addition to the imaging tools available for use in live airways.

Studies supported in part by the NH&MRC Australia, USA CF Foundation and philanthropic donors *via* Cure4CF (http://www.cure4cf.org/). SPring-8 experiments were conducted under proposal 2008B1985. Mr Paul Whiffen, Environment Manager, Boral Resources (SA) Limited, provided access to the dolomite quarry dust samples. Dr Ian Gilmour, USA EPA, supplied the combusted diesel and PM10 particulates. KSM was supported by an Australian Postgraduate Award, a Monash University J. L. William Scholarship and a Cystic Fibrosis Australia Studentship.

References

Addison, J. & McConnell, E. E. (2008). *Regul. Toxicol. Pharmacol.* **52**, S187–S199.
Cloetens, P., Barrett, R., Baruchel, J., Guigay, J. P. & Schlenker, M. (1996). *J. Phys. D*, **29**, 133–146.
Donaldson, S. H., Corcoran, T. E., Laube, B. L. & Bennett, W. D. (2007). *Proc. Am. Thorac. Soc.* **4**, 399–405.
Grubb, B. R. & Boucher, R. C. (1999). *Physiol. Rev.* **79**, S193–S214.
Grubb, B. R., Jones, J. H. & Boucher, R. C. (2004). *Am. J. Physiol. Lung Cell Mol. Physiol.* **286**, L588–L595.
Healey, F. H. & Young, G. J. (1954). *J. Phys. Chem.* **58**, 885–886.
Limberis, M., Anson, D. S., Fuller, M. & Parsons, D. W. (2002). *Human Gene Ther.* **13**, 2112.
Livraghi, A. & Randell, S. H. (2007). *Toxicol. Pathol.* **35**, 116–129.
Mery, S., Gross, E. A., Joyner, D. R., Godo, M. & Morgan, K. T. (1994). *Toxicol. Pathol.* **22**, 353–372.
Miserocchi, G., Sancini, G., Mantegazza, F. & Chiappino, G. (2008). *Environ. Health*, **7**, doi:10.1186/1476-069X-7-4.
Papirer, E. & Roland, P. (1981). *Clays Clay Miner.* **29**, 161–170.
Parsons, D. W., Morgan, K., Donnelley, M., Fouras, A., Crosbie, J., Williams, I., Boucher, R. C., Uesugi, K., Yagi, N. & Siu, K. K. W. (2008). *J. Anat.* **213**, 217–227.
Pundsack, A. L. (1955). *J. Phys. Chem.* **59**, 892–895.
Sera, T., Yokota, H., Fujisaki, K., Fukasaku, K., Tachibana, H., Uesugi, K., Yagi, N. & Himeno, R. (2008). *Phys. Med. Biol.* **53**, 4285–4301.
Snigirev, A., Snigireva, I., Kohn, V., Kuznetsov, S. & Schelokov, I. (1995). *Rev. Sci. Instrum.* **66**, 5486–5492.
Wildhaber, J. H. (2006). *Paediatr. Respir. Rev.* **7**(Suppl. 1), S86–S87.
Wilkins, S. W., Gureyev, T. E., Gao, D., Pogany, A. & Stevenson, A. W. (1996). *Nature (London)*, **384**, 335–338.
Yabashi, M., Yamazaki, H., Tamasaku, K., Goto, S., Takeshita, K., Mochizuki, T., Yoneda, Y., Furukawa, Y. & Ishikawa, T. (1999). *Proc. SPIE*, **3773**, 2–13.